Quaternary Science Reviews 302 (2023) 107961

Contents lists available at ScienceDirect

Quaternary Science Reviews

journal homepage: www.elsevier.com/locate/quascirev

Landscape constraints on mire lateral expansion

Betty Ehnvall [a, *], Joshua L. Ratcliffe [a], Elisabet Bohlin [a], Mats B. Nilsson [a], Mats G. Öquist [a], Ryan A. Sponseller [b], Thomas Grabs [c]

[a] Department of Forest Ecology and Management, Swedish University of Agricultural Sciences, Skogsmarksgränd 17, 90183, Umeå, Sweden
[b] Department of Ecology and Environmental Science, Umeå University, Linnaeus Väg 6, S-90736, Umeå, Sweden
[c] Department of Earth Sciences, Geocentrum, Uppsala University, Villavägen 16, 75236, Uppsala, Sweden

ARTICLE INFO

Article history:
Received 28 September 2022
Accepted 11 January 2023
Available online xxx

Handling Editor: Yan Zhao

Keywords:
Holocene
Landscape ecology
Boreal zone
Chronosequence
Landscape wetness
Mire lateral expansion
Non-linear
Mire available areas
Peat accumulation

ABSTRACT

Little is known about the long-term expansion of mire ecosystems, despite their importance in the global carbon and hydrogeochemical cycles. It has been firmly established that mires do not expand linearly over time. Despite this, mires are often assumed to have expanded at a constant rate after initiation simply for lack of a better understanding. There has not yet been a serious attempt to determine the rate and drivers of mire expansion at the regional, or larger spatial scales. Here we make use of a natural chronosequence, spanning the Holocene, which is provided by the retreating coastline of Northern Sweden. By studying an isostatic rebound area we can infer mire expansion dynamics by looking at the portion of the landscape where mires become progressively scarce as the land becomes younger. Our results confirms that mires expanded non-linearly across the landscape and that their expansion is related to the availability of suitably wet areas, which, in our case, depends primarily on the hydro-edaphic properties of the landscape. Importantly, we found that mires occupied the wettest locations in the landscape within only one to two thousand years, while it took mires three to four thousand years to expand into slightly drier areas. Our results imply that the lateral expansion of mires, and thus peat accumulation is a non-linear process, occurring at different rates depending, above all else, on the wetness of the landscape.

1. Introduction

Mires are ubiquitous across the boreal biome (Rydin et al., 2013) and help regulate global climate through long-term carbon sequestration and greenhouse gas exchange. These peat-forming wetlands are also important for landscape biodiversity (Joosten, 2003) and for regulating hydrological patterns and downstream water chemistry (Lane et al., 2018; Sponseller et al., 2018). To understand the role mires have had in regulating past climate and ecohydrology it is necessary to understand how they have initiated and spread across the landscape. In this context, the main requirement for persistence of undisturbed mires is a seasonally positive water balance, such that the sum of water inputs exceeds water losses (Ivanov, 1981). Climate, topography, and edaphic properties together control the water balance of the landscape, and thus, the potential for peat accumulation and mire growth (Ivanov, 1981). Indeed, strong climatic influences are manifested in the global distribution of mires within the temperature-precipitation space, which shows, for example, that higher temperatures require more precipitation to sustain significant areas of these ecosystems (Romanov, 1968; Yu et al., 2009).

Lateral expansion can take place when mire margins are waterlogged and hence made accessible for the characteristic semi-aquatic mire vegetation (Ivanov, 1981; Kulczyński, 1949; Rydin et al., 2013). Under favourable conditions, mire margins can expand several meters per year (Korhola, 1994; Loisel et al., 2013); for example, mire lateral growth could previously occur in areas that are now constrained by sloping ground (Korhola, 1996; Mathijssen et al., 2016). Despite the clear link between landscape topographical features and water balance, the most widely used (e.g. Yu et al., 2010) and recent (e.g. Nichols and Peteet, 2019) estimates of regional and global mire carbon stocks often rely on an assumption that mires expand at a linear rate after their initiation (Ratcliffe et al., 2021). This could result in substantial biases and artefacts in carbon budget estimates.

The interaction between climatic, topographic and edaphic

* Corresponding author.
E-mail address: betty.ehnvall@slu.se (B. Ehnvall).

https://doi.org/10.1016/j.quascirev.2023.107961

controls on mire development has been known for several decades and is well described in the mid-20th century literature. For example, on the west coast of Scotland annual precipitation exceeds 2500 mm, with additional occult precipitation from mist and fog (Lindsay et al., 1988). In such settings, blanket bogs are common and peat may be found on slopes as steep as 20% (Gorham, 1957; Pearsall, 1950). Moving east through Scotland, into the rain shadow of the coastal mountains, precipitation declines sharply to 650 mm or less (Lindsay et al., 1988) and peat becomes progressively confined to ever flatter areas (Gorham, 1957; Pearsall, 1950). Under such conditions, purely climatic models can accurately predict the presence or absence of blanket peat within a 2.5 km^{-2} grid (Gallego-Sala et al., 2016). In the absence of strong climatic gradients, topo-edaphic controls (topography or underlying substrate) become increasingly important for determining whether or not peat may form (Ivanov, 1981; Kulczyński, 1949). For example, with increasingly dry climatic conditions, lower terrain slopes and/or increasingly fine-textured and less permeable soils may be required to sustain a shallow water table to enable peat accumulation (Ivanov, 1981). Finally, at the driest climatic boundaries, peat formation is highly dependent on landscape position and only possible on the gentlest slopes and requires extensive lateral water inputs for initiation to occur (Kulczyński, 1949; Quick et al., 2022).

While broad-scale climate gradients are important from a global perspective, the distribution of mires within a relatively homogenous climatic space is shaped by topographical and edaphic constraints. Of these drivers, average slope (Gorham, 1957; Loisel et al., 2013), the relative proportion between the supporting watershed and the receiving mire area (Ivanov, 1981; Romanov, 1968), and hydraulic conductivity of the underlying mineral soil (Gorham, 1957; Kulczyński, 1949; Rydin et al., 2013) are all potentially important factors that control local wetness, plant species composition, and biogeochemical processes (Moor et al., 2017). It is precisely these topographic and edaphic constraints that are often overlooked in models of mire growth (Ratcliffe et al., 2021). This is despite strong evidence that the factors are of primary importance for peat initiation and lateral expansion. Understanding the temporal patterns of mire initiation, as well as the contemporary spatial distribution of mires in any landscape thus requires that we disentangle the controls of climate and topographical and edaphic factors, respectively. Conceptually, this goal is well acknowledged (Graniero and Price, 1999; Korhola, 1996; Weckström et al., 2010), yet in practice, distinguishing these controls is exceedingly difficult due to the expense and difficulty of dating peat lateral expansion across meaningful gradients of climate, soil or topographic variation.

Stronger predictive insight into mire distribution is particularly crucial for understanding the broader biogeochemical roles of these ecosystems. For example, estimates of mire carbon stocks and their development over time are commonly made with the assumption that mires have expanded at a constant rate, from a single point up to their present regional extent (MacDonald et al., 2006; Nichols and Peteet, 2019; Yu, 2011). This assumption has been criticized (Ratcliffe et al., 2021), as both circumpolar and local palaeoecological studies have indicated that peat accumulation and lateral expansion are dynamic, often reflecting shifts in Holocene climate (Loisel et al., 2014; Payne et al., 2016; Ruppel et al., 2013; Weckström et al., 2010). While these previous studies have emphasized the importance of recognizing non-linear mire lateral expansion during the Holocene, they have focused on a relatively small number of sites and hence are unable to separate site-specific conditions from regional controls. Thus, the relative importance of climatic, edaphic and topographic controls on peatland expansion is not known beyond a small handful of individual mires.

In this study, we disentangle the role of topo-edaphic controls for mire establishment and lateral expansion by investigating a c. 5500 km^2 region with ongoing land uplift, caused by isostatic rebound in northern Sweden. In areas with a clear space-for-time gradient (Walker et al., 2010), chronosequences can be used to study mire populations, as a complement to palaeoecological studies based on individual mires (Ecke and Rydin, 2000; Laine et al., 2021; Tuittila et al., 2013). Assuming that climate conditions are comparable across the region and that the transects evolved similarly over time, topo-edaphic controls should hold the key to understand local variations in mire distribution. To explore this approach, we utilized 10 chronosequences arising from isostatic rebound to estimate lateral expansion rates during the Holocene. Specifically, we used estimates of current mire cover and landscape age across the transects to test the hypotheses that mire areal increases (i) have been non-linear, and (ii) that they are associated with mire-available land areas, which are related to topo-edaphic controls. To test these hypotheses, we used isostatic displacement curves to assess when mires were established at different contemporary elevations. We then combined information on isostatic displacement curves with topo-edaphic landscape properties to evaluate the relative role of topo-edaphic controls. Our large-scale approach considers the entire mire population present in the area and fills an important gap in our overall understanding and conceptualization of mire development at the landscape scale.

2. Regional setting

During the last glacial maximum at c. 26 500–20 000 years before present (BP) (Clark et al., 2009) the entire Fennoscandia region was covered by the c. 3 km thick Scandinavian Ice Sheet, which began to retreat c. 10 000 years BP (Stroeven et al., 2016). In northern Sweden, the rate of isostatic relaxation, or rebound, slowed down over the course of this deglaciation. The current isostatic relaxation maximum of the Scandinavian Ice Sheet is located in the Swedish province of Västerbotten (c. 62–64° N), where land is rising at a rate of c. 9 mm yr^{-1} (Nordman et al., 2020). As a result, coastal areas of the Bothnian Bay region include chronosequences that span thousands of years within only tens of kilometres from the present coastline. Analogous regions with strong isostatic relaxation are found in the Hudson Bay lowlands in Canada, and in the White Sea area of Russia (Kutenkov et al., 2018; Paulson et al., 2007). In the Bothnian Bay region the direction of the retreat of the ice sheet has resulted in a landscape patterning characterized by elongated wave-exposed and till covered ridges interlaid by valleys covered by finer minerogenic deposits, mainly of silt and clay (Lindén et al., 2006). The characteristic elongated landscape features, together with the rapid net shore displacement, offers favourable conditions for mire initiation. Moving inland along these chronosequences provides a unique opportunity to explore how the size, arrangement, and connectivity of mires change over thousands of years of mire succession.

The chronosequence approach has already been successfully exploited in other regional mire studies including the Hudson Bay Lowlands (Packalen et al., 2014), and the coastal region of the Finnish Bothnian Bay area (Tolonen and Turunen, 1996; Clymo et al., 1998; Tuittila et al., 2013). The latter is notable, since the area is relatively close to our study region, and hosts a mire chronosequence of a comparable age range, and a similar spatial vegetation gradient. An early study on mires in the Finnish Bothnian Bay area revealed that approximately 60% of all mires initiated through primary mire formation (Huikari, 1956) following land uplift. This pattern indicates that the chronosequence approach should be suitable for addressing mire age at the landscape level for the majority of mires. Although the detailed contributions of

primary formation, terrestrialization, and paludification to mire genesis in the Swedish Bothnian Bay still need to be quantified, all three processes have shaped present mire patterns (Ruppel et al., 2013). At the same time, a comparison of mire age estimated from land-surface age versus age estimated from ^{14}C at three mires in this region suggests that the two approaches yield similar estimates (Fig. A2). This adds additional confidence for applying the chronosequence approach also in the western Bothnian Bay area.

3. Materials and methods

3.1. Study area

The ten investigated mire-chronosequences are located along the coastal plain of the Gulf of Bothnia (Fig. 1). The chronosequences are oriented perpendicularly to the coastline at approximately 30 km intervals. The exact positions of the areas were adjusted to exclude large rivers, as mires that have developed on floodplains greatly differ from the remaining mire population in terms of genesis and hydrology (Lane et al., 2018). The maximum elevation of a chronosequence was selected to cover a landscape age of around 0–9000 BP. Due to differences in topography and isostatic relaxation rates, the lengths of the ten chronosequences, measured as horizontal distances from the present coastline to the farthest inland border, varied from 28 to 80 km and maximum elevations varied from 130 to 190 m above the present-day sea level (m.a.s.l.). The ten chronosequences were distributed over c. 350 km along the northeastern coast of Sweden along the Kvarken and the Bothnian Bay and cover a total surface area of c. 5500 km^2. The southernmost chronosequence was delineated in the municipality of Nordmaling (63° N), north of the geomorphologically deviating High Coast area. The northernmost chronosequence was in Haparanda (66° N) by the Finnish border. Chronosequences were delimited as 10 km wide stripes of land. An exception to this is the intensively studied Sävar chronosequence, which is 24 km wide.

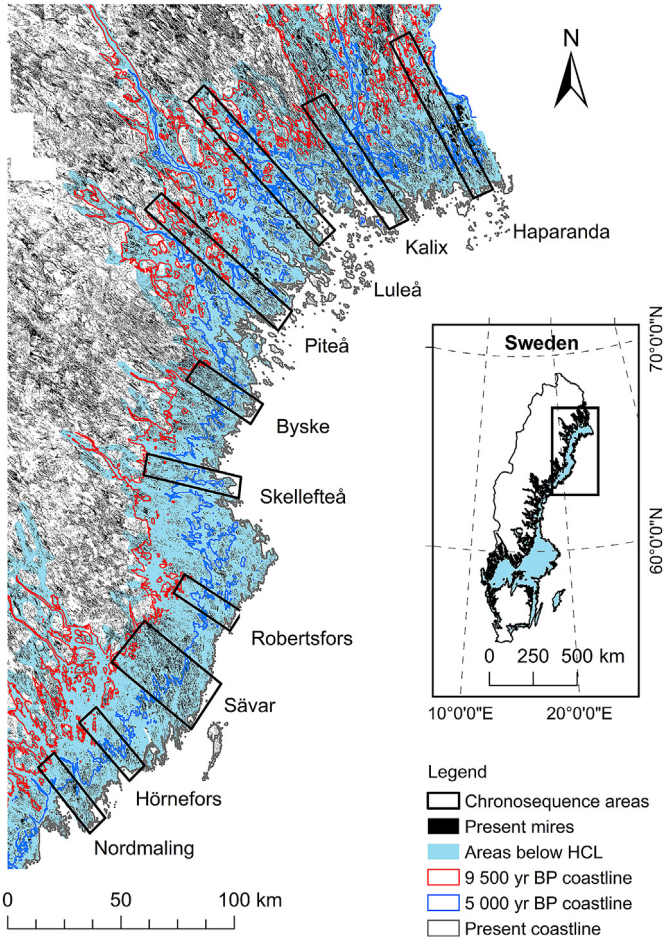

Fig. 1. Chronosequence areas along the Swedish Bothnian Bay coast are marked with rectangles. Areas below the highest coastline (HCL) are marked in blue while areas above it are marked in white. Mires, as defined in the Swedish property map (the Swedish Mapping, Cadastral and Land Registration Authority), are shown in black. Historical shorelines (© SGU) are based on models developed from empirical shore-level data and peat datings.

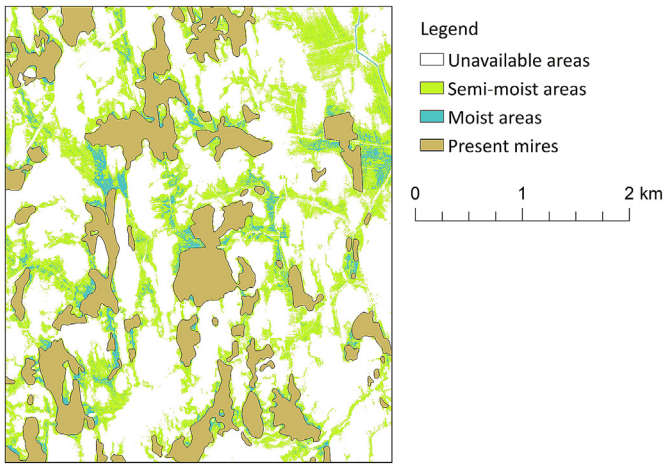

Fig. 2. Example from the Sävar chronosequence on the distribution of present mires, as well as moist mire available areas (blue, SMI >87) and semi-moist mire available areas (green, SMI >57). Moist areas are mainly found close to contemporary mires, while the semi-moist areas cover larger areas interlaying present-day mires.

All chronosequences are comparable in their geology and present climate (Table A1). Geologically, the dominant parent material is glacial till, but surface layers of postglacial clay, silt and sand deposits can be found in all chronosequences. Climatically, the 30-year average annual temperature for the 1991–2020 period ranges from 0.8 °C (Luleå inland) to 4.6 °C (Nordmaling coast), July temperatures range from 15.1 °C (Byske inland) to 16.7 °C (Skellefteå coast) and January temperatures range from −11.9 °C (Luleå inland) to −4.1 °C (Nordmaling coast). Annual precipitation ranges from 402 mm (Byske coast) to 741 mm (Nordmaling coast). According to the Swedish Wetland Survey (Gunnarsson and Löfroth, 2009) all ten chronosequences are found in the southern aapa mire subregion, which is dominated by fens (Gunnarsson et al., 2014; Gunnarsson and Löfroth, 2009). The number of individual mire objects ranges from c. 860 in Nordmaling to c. 3470 in Sävar (Table A1) and the total number of mapped, individual mires across all chronosequences is c. 18 500.

3.2. Landscape age zones

To analyze the evolution of mire properties across the ten chosen chronosequences, we subdivided each chronosequence into nine, one-millennia long, age zones. For this, we combined the Swedish national high-resolution digital elevation model (DEM) generated by Lantmäteriet (the Swedish Mapping, Cadastral and Land Registration Authority) with local shoreline-displacement curves modelled by the Geological Survey of Sweden. The 2 × 2 m DEM was derived from a LiDAR point cloud with a point density of 0.5–1 points m^{-2}, a vertical resolution of 0.3 m and a horizontal resolution of 0.1 m. The applied shoreline-displacement

curves are based on empirical data, specifically lake-tilting data, shore-level curves, tide gauge data and elevations of the highest coastline (Påsse and Daniels, 2015). Here, we estimated, landscape age (T_{age}) from elevation above sea level (z) based on second-order polynomial shoreline-displacement curves (Equation (1)) with chronosequence-specific parameters a_0, a_1 and a_2 (Table A.3):

$$T_{age} = a_0 + a_1 z + a_2 z^2 \quad \text{Eq.1}$$

The resulting landscape-age maps were further classified and vectorized into age zones spanning one thousand-year zones between 0- and 9000-years BP. Spatial analyses and cartography were performed using SAGA GIS v. 7.9.0 (Conrad et al., 2015) and ArcGIS (version 10.7.1.).

3.3. Definition of mire and land use classification

Land use data from the property map by the Swedish Mapping, Cadastral and Land Registration Authority (Lantmäteriet, 2020) was used in the study. The smallest reported mire unit was c. 2500 m^2. The property map provides currently the most detailed information on mire extent and location and also comprises information on other land use classes. In addition to identifying mire areas, we also used the property map to classify three more land-use types and to analyze their proportions within each age zone across all ten chronosequences. Selected land-use classes consisted of: (1) mires, (2) agricultural land, (3) surface waters (lakes and large streams) and (4) upland areas.

Mires in the property map were derived from aerial photos and comprise both mires isolated from larger streams as well as mires located on floodplains. Due to the adjustment of the chronosequence locations, which typically span the area in-between major rivers, floodplain mires along large rivers were present only in one of the chronosequences (Sävar, comprising in total 1.5% of the total mire area) and visually identified and manually excluded. Moreover, mires, which were artificially split by roads or ditches are shown as separate objects in the property map, were re-aggregated into single mire objects in all chronosequences.

In addition to mires, agricultural lands and surface waters were accounted for separately. Agricultural lands, including cropland and pasture, were selected as land-use class, since between 6 and 9% of the present agricultural land in Northern Sweden is located on former peat soils (Berglund and Berglund, 2010). Surface water bodies were selected as another important land-use class because of their twofold (and contrasting) influences on mire expansion. While on one hand, the presence of large surface water bodies can limit mire expansion, the presence of small surface bodies can favour mire formation through terrestrialization (Englund et al., 2013).

Finally, upland areas were defined as all remaining areas not covered by mires, water or agricultural land. According to the Swedish property map the upland areas are predominantly coniferous forests, but areas of deciduous forest, settlements, infrastructure and other open areas such as areas with vegetation height below 1.5 m, open mines and bedrock outcrops associated with water, are also found. These upland areas support mires hydrologically and are essential for mire formation and persistence and, given favourable hydrological and topographical conditions, mires can expand laterally into these areas (Ivanov, 1981; Loisel et al., 2013). Hence, all land areas except mires, agricultural areas and surface water were classified as upland areas.

3.4. Soil moisture classification

To account for varying local wetness conditions across the age zones in the ten chronosequences, we used a newly developed national soil moisture index (SMI; Ågren et al., 2021) as a proxy for topo-edaphic controls. The index is calculated using a machine-learning algorithm trained and validated on data from c. 20 000 soil plots distributed across entire Sweden. Terrain attributes at different scales, such as the topographic wetness index (Beven and Kirkby, 1979) or depth-to-water (Murphy et al., 2011), soil properties (e.g., soil depth and quaternary deposit type) as well as runoff indicators were used as input data (Ågren et al., 2021). Due to its partial dependence on the latter, the SMI is not purely topo-edaphic. However, it can be considered primarily topo-edaphic because topo-edaphic variables contributed most to the SMI (Ågren et al., 2021).

The SMI ranges from 0 to 100 based on the likelihood that a pixel in the mapped landscape is wet (0 = dry, 100 = wet). We chose two thresholds to reclassify the moisture index into three classes (moist, semi-moist, dry), with a focus on their suitability for mire expansion. The thresholds were defined as the 5th respectively 1st percentiles of soil moisture index values within present mires in each chronosequence (sorted from low to high). The 5th percentile value corresponds, hence, to the SMI value that is matched or exceeded in 95% of all mire pixels. For each chronosequence, the two thresholds were calculated and medians across all chronosequences were extracted. The median 5th and 1st percentiles correspond to moisture index scores of 87 and 57 respectively (Table 1). Here, we refer to areas with an SMI score above 87 as being moist and to areas with an SMI score above 57 as being semi-moist. Consequently, semi-moist areas also include moist areas were included since these have an SMI score above 57. Based on the moist and semi-moist thresholds we identified areas with a sufficiently high SMI for mire development, but that are not currently covered by mires (exemplified in Fig. 2).

Large, wet, homogenous areas can be less accessible for mire vegetation if they are comprised of open water bodies because terrestrialization can be slowed or impeded by deep water and wave action (Kulczyński, 1949). Since there is no simple way to differentiate open surface waters that are suitable for mire colonization from those that are not, we did not consider open surface water bodies to be mire-available through lateral expansion. Thus, we excluded all surface water from the available areas in the further analyses.

3.5. Utilization of hydrologically available land areas

Based on the semi-moist and moist land areas cumulative mire-available areas were calculated starting from the oldest inland age zone and moving towards the young present coastline. Some age zones closest to the coastal most areas had to be excluded, as soil moisture data were not available. Since SMI data were only missing in the youngest age zones, their exclusion does not affect the cumulative curves in the older parts of the landscape. All calculations, statistical analyses and data visualization were carried out using R version 4.0.3 (R Core Team, 2020; Vienna, Austria).

To further study the landscape age effects on mire utilization of available areas, we performed a series of Kendall's rank correlation tests to visually evaluate indications for the existence (and temporal persistence) of a relationship between landscape age and the percentage of mire area per available moist or semi-moist areas. For this, we successively increased the number of age zones included in the correlation analysis, starting from the two youngest age zones.

3.6. Normalization of present-day mire area to potentially available areas

To compare mire lateral expansion across all ten

Table 1
Mire moisture probabilities (%) were calculated from the national soil moisture map (Ågren et al., 2021). Chronosequence specific soil moisture scores corresponding to the 5th and 1st percentiles are presented for each chronosequence, together with the median, mean and standard deviation across all chronosequences.

Chronosequence	Moist areas (5th percentile)	Semi-moist areas (1st percentile)
Haparanda	95	81
Kalix	87	55
Luleå	87	51
Piteå	86	57
Byske	93	73
Skellefteå	87	60
Robertsfors	87	55
Sävar	93	73
Hörnefors	84	57
Nordmaling	84	52
Median	87	57
Mean	88.3	61.4
Std dev	3.7	9.9

chronosequences ($c = 1 \ldots 10$), we derived the cumulative mire area $y_{cj,k}$ relative to the total mire area of each chronosequence. The cumulative mire area was calculated as the cumulative sum of mire areas $a_{mire,c,i}$ within each age zone starting from the oldest (farthest inland) age zone ($i = 1$) and moving towards younger (more coastal) age zones ($i = k$) (Eq. (2)).

$$y_{c,k} = \sum_{i=1}^{k} a_{mire,c,i} / \sum_{i=1}^{10} a_{mire,c,i} \quad \text{Eq. 2}$$

While the metric $y_{cj,k}$ (Eq. (2)) has the advantage of being simple, it does not account for potential bias introduced by differences in the areal extent of age-zones. The latter can result from variable isostatic relaxation rates and variable, large-scale slope across the chronosequences. To compensate for this potential bias, we derived an adjusted cumulative mire-area percentage by rescaling age-zone mire area $a_{mire,c,i}$, based on the corresponding age-zone $a_{c,i}$, and average age-zone area $\overline{a_c}$ (Eq. (3)).

$$y_{area,c,k} = \sum_{i=1}^{k} \left(a_{mire,c,i} \cdot \frac{\overline{a_c}}{a_{c,i}} \right) \Big/ \sum_{i=1}^{10} \left(a_{mire,c,i} \cdot \frac{\overline{a_c}}{a_{c,i}} \right) \quad \text{Eq. 3}$$

Since not all areas within an age-zone can be considered equally suitable for mires, we further calculated cumulative mire areas percentages relative to the occurrence of semi-moist $a_{semi,c,i}$ and moist areas $a_{moist,c,i}$, respectively. Similar to before, we rescaled mire area using the ratio of mean to age-zone-specific suitable areas (i.e., $\overline{a_{semi,c}} \cdot a_{semi,c,k}^{-1}$ and $\overline{a_{moist,c}} \cdot a_{moist,c,k}^{-1}$) and normalized by total semi-moist (A_{semi}) and moist areas A_{moist} (Eq. (4) and *5) respectively.*

$$y_{semi,c,k} = \sum_{i=1}^{k} \left(a_{mire,c,i} \cdot \frac{\overline{a_{semi,c}}}{a_{semi,c,i}} \right) \Big/ \sum_{i=1}^{10} \left(a_{mire,c,i} \cdot \frac{\overline{a_{semi,c}}}{a_{semi,c,i}} \right) \quad \text{Eq. 4}$$

$$y_{moist,c,k} = \sum_{i=1}^{k} \left(a_{mire,c,i} \cdot \frac{\overline{a_{moist,c}}}{a_{moist,c,i}} \right) \Big/ \sum_{i=1}^{10} \left(a_{mire,c,i} \cdot \frac{\overline{a_{moist,c}}}{a_{moist,c,i}} \right) \quad \text{Eq. 5}$$

4. Results

4.1. Mire area distribution

Present-day mire coverage and absolute area varied both in magnitude and spatial distribution over age zones (Fig. 3). The maximum mire coverage of 44%, within any age zone, was found in Haparanda, the northernmost chronosequence, at c. 4000–5000 years BP. In contrast, Robertsfors had the lowest mire coverage of all chronosequences, only reaching a maximum mire coverage of 16%. Yet, there was no apparent latitudinal gradient in total mire coverage overall. In many of the chronosequences, such as Haparanda, Sävar, Nordmaling and Hörnefors, mire coverage was high in the landscape age zones representing primary mire initiation during the mid-Holocene (c. 5000–3000 years BP). Peaks in mire coverage, in the Mid-Holocene landscape age zones, in Luleå and Robertsfors were only modest, while in other areas like Skellefteå and Kalix the lowest mire coverage was found in age zones released during the mid-Holocene. Byske was unique in its almost linear increase in mire coverage with landscape age.

All of the studied chronosequences contained agricultural land within the individual age zones, on average 4.3% (SD 5.5%). The highest proportions of agricultural land were found in the coastal and central parts of the Robertsfors and Hörnefors chronosequences (25% and 24% respectively). We estimated the potential influence of mire drainage for agricultural purposes in each chronosequence by comparing the coverage of agricultural lands to moist and semi-moist land areas in each age zone using the non-parametric Kendall's rank correlation test (Table A.4). Across all chronosequences, we found low and non-significant Kendall's Tau correlation coefficients of Tau < -0.01 for moist areas and Tau <0.01 for semi-moist areas. Therefore, agricultural drainage did not introduce systematic bias into our results. Since Robertsfors was one of the chronosequences with the highest coverage of agricultural land (Fig. A1) and at the same time is likely to be affected by concomitant mire drainage, the mire expansion patterns in the area might be more notably diminished due to agricultural activities compared to the other chronosequences. Open surface waters were found in all age zones of the studied chronosequences ranging from 0.05 to 27% of the total area within the age zones of each chronosequence.

4.2. Distribution of contemporary mire area and land areas suitable for mire establishment

The distribution of current mire area and potentially available

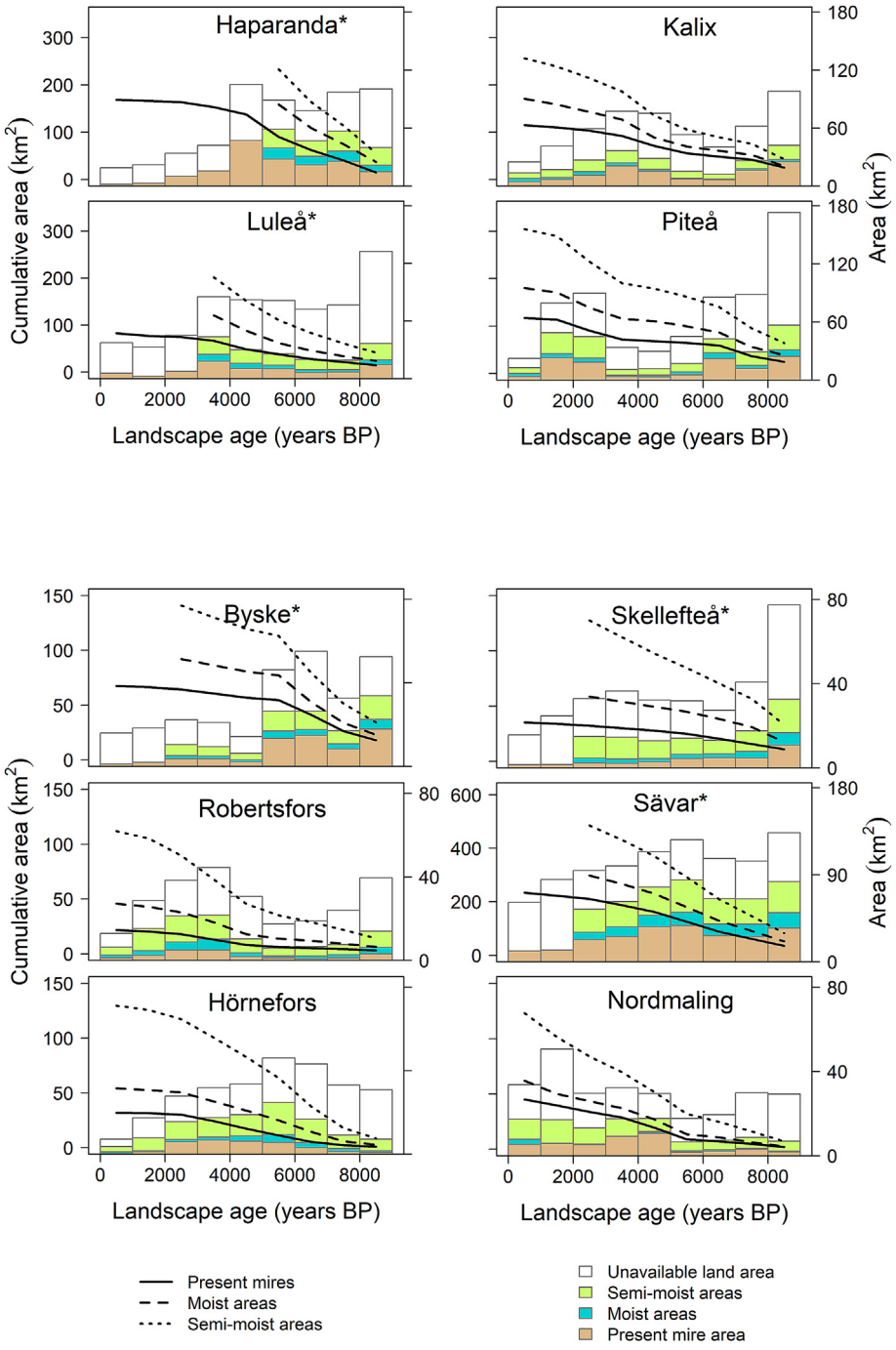

Fig. 3. Cumulative areas of current mires (solid line), as well as moist (dashed line) and semi-moist land areas (dotted line). The plots of the four northmost chronosequences were grouped, and have identical primary and secondary vertical axes ranges of 0–350 km^2 and 0–180 km^2, respectively. Correspondingly, the plots of the six southern chronosequences were grouped, and have primary and secondary vertical axes ranges of 0–150 km^2 and 0–80 km^2, respectively. An exception is the (wide) Sävar chronosequence with primary and secondary vertical axes ranges of 0–600 km^2 and 0–180 km^2, respectively. Stacked bars in the background show the present mire area (brown), available moist areas (blue), available semi-moist areas (green), and unavailable areas (white.) Age zone areas missing soil moisture index data in the younger age zones are highlighted with an asterisk, and only mire area and total area information are shown for these age zones.

areas, i.e. moist and semi-moist areas across the age classes differed between chronosequences (Fig. 3). Many of the chronosequences exhibited non-linear changes in the age-class-specific mire proportions around mid-Holocene (4000–5000 years BP). However, some changes in trends were associated with an increase in the slope of the cumulative mire area (e.g. Hörnefors and Nordmaling), while other changes were associated with decreases (e.g. Byske). The changes in slopes corresponded to changes in age zone areas, as represented by the bars in the background (Fig. 3).

If a specific age zone is larger or smaller as compared to an adjacent younger age zone, then this will be manifested as differences in the slope of the accumulated curve of potential or current mire areas. In order to account for varying mire areas resulting from differences in exposed land areas, we use the mire coverages instead of the absolute mire areas later on in the analysis.

4.3. Actual and potential mire coverage across age zones

The proportion of potentially available land areas (moist and semi-moist areas) currently covered by mires varied considerably within age classes in the chronosequences (Fig. 4). In all age classes, potentially available land area exceeded the actual coverage of contemporary mires. The large variability in the discrepancy between contemporary mire coverage and potentially mire-available areas can be seen in the gap between the potential mire area and the actual mire area. For example, for a 50% mire availability of semi-moist land areas, the actual mire coverage ranged between c. 5% and c. 30%.

Importantly, both in old (Fig. 4a, red points) and young (Fig. 4a, blue points) age zones the utilization of available moist land areas was relatively high, which might indicate that mire expansion to the wettest part of the landscape occurred within c. 2000 years (Fig. 4). Lateral expansion into semi-moist parts of the landscape, in turn, appears to be related to landscape ageing. Older age zones (Fig. 4b, red points) were found closer to the marked 1:1 line, while younger age zones (Fig. 4b, blue points) were further apart from the 1:1 line.

Generally, contemporary mires occupied 70–80% of the available moist land areas throughout the chronosequences (Fig. 5a). Only in the youngest 0–1000 year BP age zone, mire utilization of available moist areas was lower than 60%. For semi-moist areas, we observed a slow, yet continuous, increase in mire utilization of available areas over the first four age zones (Fig. 5c). These are indications that mire lateral expansion into semi-moist areas may have slowed down during the mid-Holocene. We found decreasing Kendall's Tau coefficients for moist areas as we increased the number of age zones from young to old, and correspondingly, only the first two correlations (i.e. 0-2000 years BP: $p < 0.05$ ($n = 20$) and 0–3000 years BP: $p < 0.1$ ($n = 30$); Fig. 5b) were significant. For semi-moist areas, the Tau correlation coefficient decreased after c. 4000 years (from young to old). For semi-moist areas, only the first correlation (0–2000 years BP) was significant at $p < 0.1$ (Fig. 5d).

4.4. Cumulative mire areal increase

There was a considerable variation in the distribution of relative coverage of contemporary mire area between age classes throughout the ten studied chronosequences, as illustrated by the curves on normalized cumulative mire area (Fig. 6a). In the Byske chronosequence, for example, the mire population was dominated by old mires and 50% of the mire area were located on areas older than c. 7500 years BP. In contrast, 50% of the mire area in Nordmaling were located on areas older than c. 4500 years BP. None of the chronosequences had a constant expansion rate in cumulative mire area over age zones, with more pronounced (e.g., Robertsfors) or less pronounced (e.g., Sävar) shifts in the cumulative mire area.

However, the cumulative sum of mire area normalized to the total chronosequence specific land area (Fig. 6a) were strongly influenced by absolute areal differences between age zones, and thus, by the total area available for mire growth. After rescaling the cumulative mire area curves to total area within each age zone (Equation (3)), the apparent differences between the ten chronosequences decreased markedly (Fig. 6b), but still displayed substantial differences between chronosequences. Characteristic trends in lateral expansion remained prominent when mire area was normalized to the total age zone area (Fig. 6b). For instance, chronosequences dominated by old mires (eg. Byske and Skellefteå) remained so after rescaling to the total age zone area, while chronosequences characterized by younger mires (eg. Nordmaling and Robertsfors) remained younger after re-scaling. Differences between age zones further decreased following normalization to semi-moist and moist areas within each age class (Equations (4) and (5)). Especially in the latter two cases, the cumulative areal increase along the Sävar chronosequence was close to constant (Fig. 6c and d). Apart from Sävar, all chronosequences approached equilibrium, i.e. close to zero expansion resulting in straight cumulative curves after mire area was normalized to available moist areas.

5. Discussion

As hypothesized, we found (i) mire lateral expansion was non-linear with (ii) differing expansion rates associated with differences in potentially mire-available land areas. Moist locations were rapidly occupied by mires within c. 2000 years after land exposure

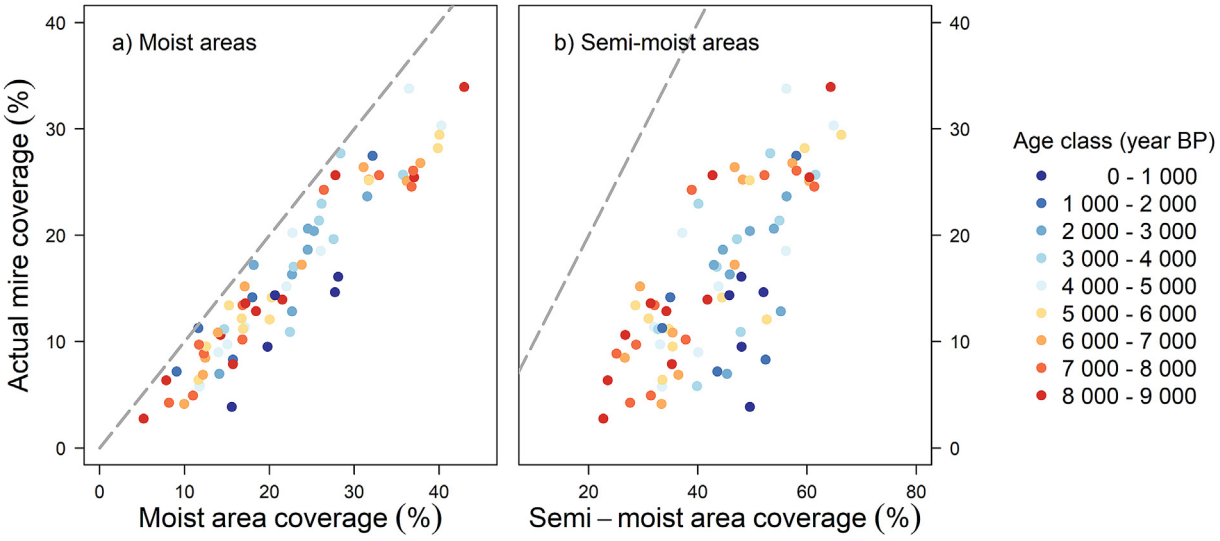

Fig. 4. Contemporary mire coverage compared to the available land areas across the ten chronosequences. Points represent individual age zones and are coloured according to the zone age. For interpretation, the 1:1 line is shown, which corresponds to a hypothetical scenario where all hydrologically available land areas are covered by mires. Deviation from the line demonstrates how large areas are still mire available in the individual age zones. Age zones with missing wetness data are not included in the figure.

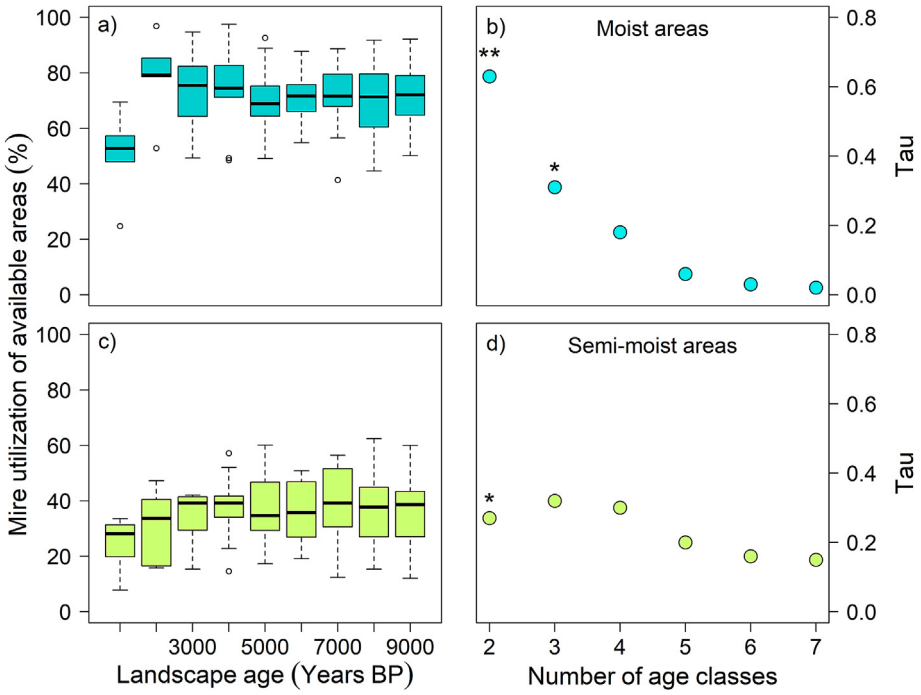

Fig. 5. Mires effectively utilize moist available land areas throughout the chronosequences (a); c. 70–80% of all areas are occupied by mires. Only in the youngest age zone (0–1000 years BP) mire utilization of available areas is lower than 60%. Landscape age effect on mire utilization of available land areas is more prominent in semi-moist areas (c), where an increased landscape age leads to higher utilization of available areas. The strength of the relationship between landscape age and mire utilization of available areas is represented by Kendall's Tau correlation coefficients between landscape age and mire utilization of available areas (%) for moist (b) and semi-moist (d) areas respectively. Kendall's rank correlation test was performed for an increasing number of age zones, starting with two age classes. Significant correlations are indicated as $p < 0.05$ (**) and $p < 0.1$ (*).

from the sea, as we inferred by the difference in mire extent in these areas across the chronosequences. In contrast, for semi-moist areas, mire coverage increased at a slower rate, since the utilization of semi-moist areas stabilized only after c. 4000 years (Fig. 5). In these areas, the rate of vertical growth and lateral expansion resulting from it, likely determine how large areas are covered by mires under the contemporary hydrologic regime. Vertical peat accumulation is a prerequisite for a rise in the absolute water table, gradually modifying the wetness of surrounding land, including through clogging the pores of the soil with particulate matter originating from the peat itself (Rydin et al., 2013), thus creating the conditions through which peat can form on mineral soil.

The high proportion (c. 50%) of moist areas covered by mires in the youngest age zone (0–1000 years BP) followed by an increase to c. 80% in the second youngest age zone (1000–2000 years BP) point towards a relatively rapid expansion of peat into suitably moist areas. We conclude that there is no considerable increase in mire expansion into moist available areas after c. 2000 years BP (Fig. 5). Since the total area of moist areas in the youngest age zone was on average 750 ha, the corresponding mire expansion rate based on our approach is approximately 0.4 ha yr^{-1} per chronosequence. Others have also observed rapid expansion rates of peat for individual mires, via paludification, in connection to very flat and wet terrain. For instance, a mire expansion rate of 0.1 ha yr^{-1} was reported for a mire in Finland (Korhola, 1994). Linear expansion rates reported elsewhere range from 3 to 8 m yr^{-1} (Loisel et al., 2013; Mäukiläu, 1997; Peregon et al., 2009; Pluchon et al., 2014) with estimates as high as tens of meters per year anecdotally reported by Ivanov (1981). Our estimate is also consistent with the potential for rapid terrestrialization of lakes, which can occur at a similar rate, for example, 3.9 m lateral ingrowth yr^{-1} in Northern Sweden (Sannel and Kuhry, 2011).

Unlike earlier studies, our data show not only that rapid initiation and spread is possible, but also that rapid expansion into wet sites has been common during the last millennium, as evidenced by the consistency across chronosequences (Fig. 5). It is worth noting that the rapid expansion of mire in response to relatively wet conditions, does not necessarily favour the rapid colonization of these areas after deglaciation or, as in our case, emergence from the sea. Peat formation could lag land availability considerably if substrate conditions were initially unsuitable (e.g. Gorham et al., 2007), if the plant dispersion rates or productivity were slow (Sundberg et al., 2006; Tiselius et al., 2019), or if the climate was historically dryer (e.g. Morris et al., 2018).

Our data show that mire extent and coverage stabilized after about 4000 years (Fig. 5). It is, however, important to note that the chronosequence approach used here cannot say for certain when mire expansion occurred, only that land suitable for mire colonization also appears to be occupied by mires to a similar degree after about 4000 years. This implies that the availability of wet environments becomes limiting to mire growth after this time. For further lateral expansion, an increase in wetness is necessary. Potentially, this can happen due to climate change, but it is unlikely to occur due to autogenic processes linked to vertical growth. This is consistent with earlier case studies from the Nordic region, which have found mires in Finland and the north of Sweden to be constrained by their surrounding topography and to be expanding very little, or not at all, in the present day (Korhola, 1994; Malmström, 1923; Weckström et al., 2010). Possible exceptions to this are mid-Holocene mires located on very flat terrain in central Sweden (Foster et al., 1988; Foster and Jacobson, 1990). Despite the limitations of our approach, the similarity of behaviour across chronosequences (which span a latitudinal gradient of ca 350 km) suggests that peat expansion in comparable climate conditions is

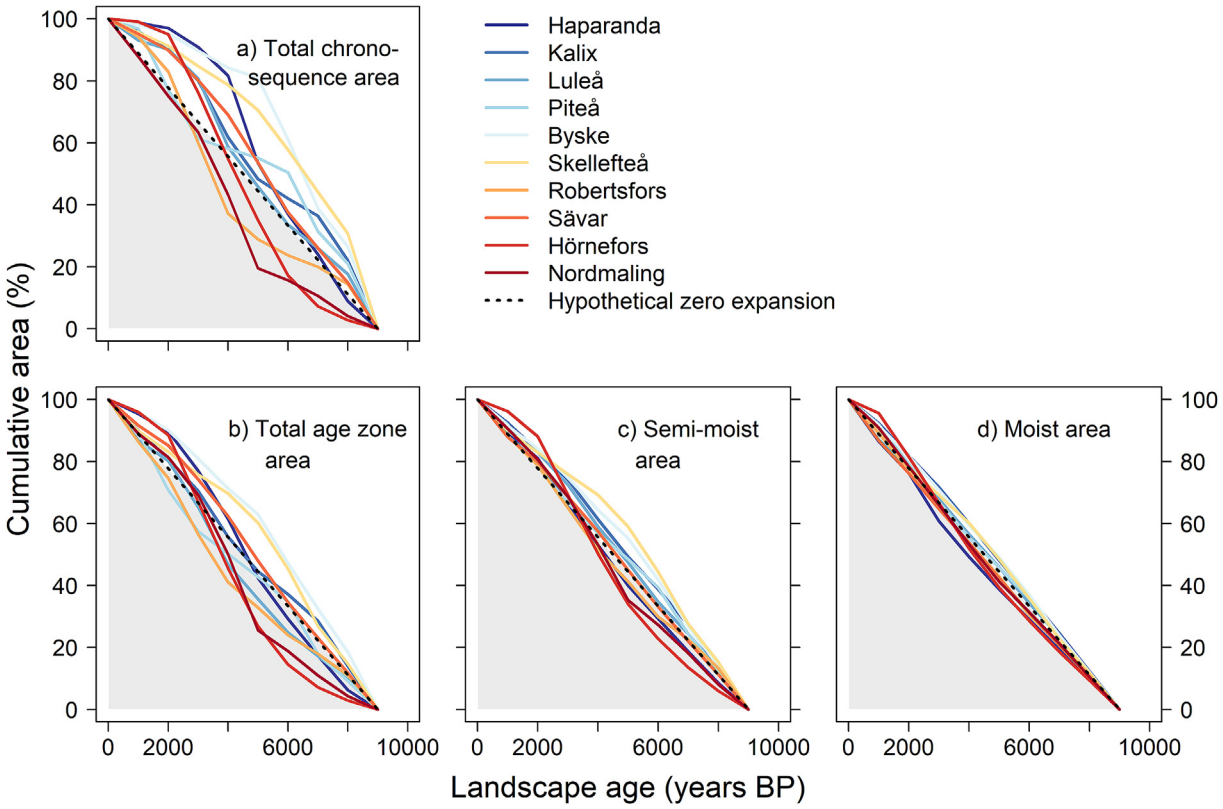

Fig. 6. Cumulative mire area, normalizations relative to a.) total chronosequence specific land area, b.) specific age zone area, c.) semi-moist areas and d.) moist areas within the age zones. When equally large mire areas are added for each age class, i.e. no lateral expansion occurs, cumulative mire area results in the marked hypothetical zero expansion line. Chronosequences above the line experience larger areal increase in older age zones, due to constant lateral expansion rate, but increased mire area over time or because of faster mire lateral expansion in older age zones. Chronosequences below the hypothetical zero expansion curve, in the grey shaded area, experience faster lateral expansion in young or intermediate age zones compared to older age zones.

occurring in the moist locations, similar to patterns reported by Korhola (1994) for an individual wet and flat mire, but in contrast to another mire system on permeable and sloping ground where climate-driven variation in wetness led to changes in the expansion rate (Korhola, 1996).

It is interesting to note that neither the moist nor the semi-moist areas can approach 100% occupation by mires, with the proportion stabilizing at c. 80% and c. 40% respectively. There are several possible explanations for this observation. While the moisture index outperforms all other currently available alternatives for estimating soil wetness in Sweden (Ågren et al., 2021) there are still be some uncertainties in the model drivers, for instance, regarding soil permeability. In addition, the forest landscape of northern Sweden has been drained for forestry since the late 1800s. It is important to note that ditches have influenced the soil moisture map by altering surface flow paths, but also that ditches have influenced the mire area itself. It is not possible to estimate the extent of influence of forest ditches on the soil moisture index, but they are undoubtedly captured by it. Aside from this, there is a natural element of bi-stability between the mires and forest landscapes, with each capable of occupying the same locale in the landscape and modifying conditions to suit their own growth (Ohlson et al., 2001; Ratcliffe et al., 2017; Velde et al., 2021). Mires in relatively flat areas can modulate their surroundings and change the landscape hydrology as a part of the paludification process (Ivanov, 1981; Kulczyński, 1949; Rydin et al., 2013). In areas drained for forestry purposes, the overlap in suitable areas between forests and mires can be even wider compared to pristine areas. An analogous situation may also exist for agricultural land. There is a significant overlap in areas where mires might have existed and areas that are currently, or have in the past been farmed. Mires could have been either prevented from forming (e.g. Tipping, 2008), or else may have been drained for agricultural activities. However, based on our results, we conclude that the overall effect of mire drainage for agricultural purposes is small in the study area, but within the chronosequences, mire drainage for agriculture is more widespread in Piteå, Robertsfors and Luleå compared to the other studied chronosequences (Table A4). Furthermore, primary mire initiation is widely understood to be a different process than paludification (Ruppel et al., 2013), requiring greater inputs of water from the surrounding upland (Ruppel et al., 2013). Pockets of moist or semi-moist land that are suitable for paludification may exist, but lack the specific locales that have continuous oversaturation of upper soil horizons necessary for primary peat formation to occur (Ivanov, 1981; Kulczyński, 1949; Malmström, 1923; Rydin et al., 2013).

It is tempting to compare the soil moisture thresholds we describe here as moist and semi-moist with empirical data on soil moisture content and speculate how this affects the redox state and thus the decay of organic matter (Husen et al., 2014; Lafleur et al., 2005). However, the wet conditions as defined by the soil moisture index are based on somewhat coarse measures of soil moisture derived from the Swedish National Forest Inventory relying on the plant community and the wetness underfoot (Ågren et al., 2021).

While it is not possible to directly translate the soil moisture index into a plausible range of soil moisture conditions, there is a clear positive relationship between the thickness of the organic layer and the soil moisture index above 60% (Ågren et al., 2022), remarkably similar to the semi-moist threshold of SMI >57 derived here from our data. It thus seems likely that this moisture index threshold also corresponds to a threshold for the occurrence of peat-forming plants and limited organic matter decomposition, but this would require further work to confirm. Despite this, our results clearly support earlier assertions about the important role of soil moisture in determining peat expansion rates. It is usually not possible to measure soil moisture conditions prior to peat formation, since mires, by their very nature, modify soil moisture conditions after they initiate (Ivanov, 1981; Rydin et al., 2013). In our case, we were able to determine past wetness conditions retrospectively by assessing where mires are missing in the younger parts of the landscape, relative to the older locations.

Although, we consider topo-edaphic conditions to be the dominant control of wetness and thus mire lateral expansion, climate has doubtlessly also influenced mire coverages across the studied chronosequences over long time periods, as has been found elsewhere (Graniero and Price, 1999). Given favourable conditions, mires can expand rapidly, as we found for our moist locations, but may expand only very slowly or not at all, under less favourable conditions, for example on slopes, during drier climate periods, or on well-drained soils as we found for our semi-moist locations (Fig. 5; Almquist-Jacobson and Foster, 1995; Gorham, 1957; Graniero and Price, 1999). Mire expansion slows or halts as slope increases and the soil becomes better drained (Almquist-Jacobson and Foster, 1995; Graniero and Price, 1999; Loisel et al., 2013; Piilo et al., 2020; Pluchon et al., 2014) and expansion generally occurs quicker on impermeable substrates, such as clay compared to more permeable ones (Korhola, 1996). The reverse is also true: mires can expand rapidly when wetness increases due to climate (Korhola, 1996; Morris et al., 2018), tectonic changes (Ivanov, 1981; Lähteenoja et al., 2012; Morris et al., 2018), or pedogenic processes such as the formation of impermeable iron pan soils (Gorham, 1957; Gorham et al., 2012; Rydin et al., 2013).

During unusually wet phases of climate, mires may expand onto dry ground previously unsuitable for peat formation and this process can be essentially one way, providing there is enough time for a layer of peat with low hydraulic conductivity and transmissivity to form (Ivanov, 1981). Such episodic expansion, linked to wet phases, has been found to occur (Korhola, 1996; Turunen and Turunen, 2003), for instance, when peat expanded rapidly during the mid-Holocene even over sandy sloping soils (Korhola, 1996). Episodic expansion of individual mires in our study area cannot be excluded, since the chronosequences approach does not say for certain when individual mires have formed. However, a comparison of mire ages based on the land surface elevation and peat ^{14}C dating (Fig. A2.) revealed a linear relation between elevation and peat age, which indicates that our approach indeed can capture differences in mire age at the landscape level. Even if episodic peat expansion has occurred in the area, the core message of our results remains the same, since we primarily compare the utilization of available wet areas across the individual landscape age zones. In addition to long-term climate variation, our studied chronosequences vary when it comes to the present climate, for example, annual temperature and precipitation vary between and within the chronosequences (Table A1). However, present-day climate differences in the study area are negligible given the bioclimatic envelope of boreal mires (Yu et al., 2009). Hence, we consider topo-edaphic constrains to be predominant driver of soil wetness and thus lateral expansion in the area, with Holocene climate playing a minor role, as illustrated by increasingly linear expansion rates as wetter landscape positions conditions are considered (Fig. 6).

Based on our results we outline three possible patterns of mire lateral expansion in the study area (Fig. 6). If equally large mire areas had occurred in each age class, the cumulative mire curves would be linear, indicating zero-lateral expansion pattern (Fig. 6, zero-expansion line). Here, we found that the chronosequences approached close to zero expansion after mire area was rescaled to available moist areas. In such cases, the cumulative growth in mire area occurs mainly due to isostatic rebound and the emergence of "new" land from the sea. This implies that mire expansion into the wettest areas of the landscape can be very rapid. In a hypothetical landscape with no landscape constraints and constant peat accumulation rates, cumulative mire area will increase more slowly in younger age classes and faster in older age classes because of the increasing mire area over time, while the actual rate of lateral expansion in each edge point remains the same. This second pattern is characterized by cumulative curves above the hypothetical zero expansion line (Fig. 6, light region). After normalization to the total available land areas two out of ten studied chronosequences follow this pattern (Byske and Skellefteå; Fig. 6b). Finally, the third possible pattern can theoretically be related to changed expansion rates in each edge point over time. If mire lateral expansion was initially fast, but gradually slowed down over the Holocene, the cumulative curve would be found below the hypothetical zero expansion curve. Reasons for this third possible pattern could, for example, be higher primary productivity in young nutrient rich stages favored by warmer or wetter conditions (MacDonald et al., 2006). Three out of the ten chronosequences follow this pattern after normalization to the total land area per age zone (Robertsfors, Hörnefors and Nordmaling). The remaining five chronosequences show patterns with curves oscillating around the hypothetical zero expansion curve.

In addition to advancing our understanding of the major controls of lateral peat expansion, these results also have important implications for the way developments in mire carbon stocks and methane emissions during Holocene are calculated. Global peatland carbon stocks are most commonly estimated using the time-history approach (e.g. Loisel et al., 2017; MacDonald et al., 2006; Nichols and Peteet, 2019; Yu et al., 2010). Following this approach, annual carbon sequestration rates are applied to a model of peatland area development throughout time. The accuracy of these carbon stock estimates is, thus, dependent on accurate estimates of historical peatland cover (Ratcliffe et al., 2021). Peatland area is modelled from basal radiocarbon dates, with the oldest assumed to represent peatland initiation. After this time, peatlands are then assumed to expand at a constant rate until they reach their present modern-day extent, following a pattern of linear growth at the regional scale. Thus a rapid expansion of peatland area favours a larger carbon sink and *vice versa*. One major problem with this approach is that mire expansion is not constant, rather topography, climate and soil properties come together to place limits on mire lateral growth as shown here at the large-scale and elsewhere for individual mires (Gorham et al., 2012; Graniero and Price, 1999; Korhola et al., 2010; Loisel et al., 2013; Weckström et al., 2010).

If a non-linear expansion rate reflecting local topo-edaphic and climatic conditions would instead be considered, both the estimated mire development state and the maximum possible carbon storage would likely be affected. Understanding other ecosystem services, such as landscape biodiversity (Joosten, 2003), and

regulation of landscape ecohydrology and downstream water chemistry (Lane et al., 2018; Sponseller et al., 2018) can also be affected by the long-term, non-linear lateral expansion of mires. While peat expansion was rapid at the moist sites in our study, these locations comprise a comparatively small part of the landscape. Thus, the slower, more variable rate of expansion associated with the drier 'semi-moist' locations could be of greater relevance for the rate of expansion over the Holocene, and the associated implications for key properties of mire ecosystems.

6. Conclusions

In this large landscape-scale study, we demonstrate how mire lateral expansion in northern Sweden is controlled by local landscape settings. We found that mire expansion occurred rapidly in moist locations (within 1000–2000 years), while drier, semi-moist areas were colonised at a much slower rate, and became occupied after about 4000 years. As such, the rate of mire expansion in our study area was highly dependent on the local soil wetness, which in turn is primarily controlled by topo-edaphic landscape conditions. Accounting for these conditions enabled us to detect comparable peat expansion behaviours across wide areas, which otherwise would have seemed to be rather heterogeneous and site-specific. This work demonstrates how we, by taking landscape constraints into account, can achieve more realistic projections of mire lateral expansion, compared to commonly assumed linear mire expansion rates. Our novel large-scale approach to assess mire lateral expansion is an important step in being able to scale up various mire properties to the landscape scale and conceptualize mire development over the Holocene time-scale.

Author contributions

B.E., J.R., M.B.N. and T.G. conceived and conceptualized the study. B.E and T.G designed the methodology, B.E. gathered the data and performed the analyses. B.E, J.R. and M.B.N. wrote the first draft. All authors interpreted and discussed the ideas and results, and contributed to writing the final manuscript.

Declaration of competing interest

The authors declare that they have no known competing financial interests or personal relationships that could have appeared to influence the work reported in this paper.

Data availability

Data will be made available on request.

Acknowledgements

This work was primarily funded by the Swedish Research Council Formas [2016–00896] and [2020-01436], with supplementary support from the Swedish Nuclear Fuel and Waste Management Company (SKB). The authors would also like to thank Anneli Ågren and William Lidberg for their insightful comments about the soil moisture index.

Appendix

Table A.1
Mire chronosequence attributes related to geography, climate (averages for 1991–2020) and geology. Chronosequence-wide mire coverage (%) and abundance (nr/km^2) is provided along with the total number of mires in parentheses. Temperature and precipitation ranges are shown for the weather station closest to the center of the present coastline, and, in parentheses, for the weather station closest to the oldest inland border of each chronosequence. The weather stations are provided in Table A.2. Abbreviations for the dominant rock type correspond to GP = granite, pergamitite, M = metagreywacke, mica schist, graphite- and/or sulphide-bearing scist, paragneiss, migmatite, quartzite, amphibolite and C = granitoid and subordinate syenitoid.

Chrono-sequence	Centroid Latitude	Centroid longitude	Coverage[5] [% mire]	Abundance[1 and 5] [nr mire/ km^2]	Length [km]	Elevation[2 and 5] [m.a.s.l.]	T_{Annual}[3] [°C]	T_{July}[3] [°C]	T_{Jan}[3] [°C]	P_{Annual}[3] [mm]	P_{July}[3] [mm]	P_{Jan}[3] [mm]	Rock[4]
Haparanda	66° 06′ 25″ N	23° 39′ 16″ E	25	2.3 (1706)	76	140	2.5 (1.6)	16.3 (15.8)	−9.2 (−11.1)	608 (625)	50 (77)	60 (47)	GP
Kalix	65° 58′ 32″ N	22° 45′ 36″ E	21	4.1 (2602)	60	130	2.6 (1.5)	15.7 (15.9)	−8.5 (−11.4)	613 (602)	61 (74)	47 (45)	M
Luleå	65° 59′ 47″ N	21° 51′ 21″ E	12	3.5 (2786)	80	130	1.5 (0.8)	15.8 (15.0)	−11.4 (−11.9)	620 (539)	71 (79)	51 (35)	GS
Piteå	65° 38′ 09″ N	21° 21′ 18″ E	17	3.3 (2575)	75	170	2.9 (1.5)	16.3 (16.0)	−8.5 (−11.7)	601 (552)	68 (90)	50 (37)	GS
Byske	65° 07′ 04″ N	21° 16′ 49″ E	24	3.7 (1162)	31	170	3.4 (2.4)	15.3 (15.1)	−6.2 (−8.0)	402 (687)	52 (90)	20 (50)	M
Skellefteå	64° 47′ 57″ N	20° 54′ 22″ E	11	4.3 (1477)	41	170	3.8 (3.2)	16.7 (15.9)	−6.9 (−7.4)	591 (600)	74 (80)	43 (42)	M
Robertsfors	64° 17′ 36″ N	20° 56′ 14″ E	9	3.5 (944)	28	190	3.6 (3.3)	15.5 (15.7)	−6.3 (−6.9)	670 (632)	66 (80)	50 (44)	M
Sävar	64° 00′ 28″ N	20° 30′ 49″ E	25	3.3 (3469)	47	170	3.9 (3.0)	16.0 (15.4)	−6.2 (−7.4)	672 (635)	69 (89)	52 (43)	M
Hörnefors	63° 46′ 05″ N	19° 57′ 60″ E	11	3.0 (927)	33	170	3.9 (3.1)	16.0 (15.4)	−6.2 (−7.2)	672 (685)	69 (84)	52 (54)	M
Nordmaling	63° 35′ 06″ N	19° 34′ 34″ E	16	2.8 (860)	35	170	4.6 (4.1)	15.9 (15.7)	−4.1 (−5.4)	714 (539)	60 (82)	35 (54)	M

[1] Mire units based on mires as defined in the Swedish property map (the Swedish Mapping, Cadastral and Land Registration Authority). The total number of mires is provided in brackets.
[2] Maximum elevation of chronosequence.
[3] 30-year average temperature and precipitation for weather station closest to the center of the present coastline, as well as the station closest to the oldest inland border in brackets. Data from the Swedish Meteorological and Hydrological Institute.
[4] Data from the Geological Survey of Sweden.
[5] Data from the Swedish Mapping, Cadastral and Land Registration Authority.

Table A.2
30-year average temperature and precipitation data used to describe the mire chronosequence climate originate from the sites named in the table (the Swedish Meteorological and Hydrological Institute). Coordinates are given as Sweref TM. For Skellefteå two different coastal climate stations were used, since only temperature data was available from the more coastal station (Ursviken). Hence, precipitation data for the coastal parts of the Skellefteå chronosequence originate from the climate station called Skellefteå.

Chrono-sequence	Coastal climate station				Inland climate station			
	Name	North	East	Elevation	Name	Lat.	Long.	Elevation
Haparanda	Haparanda	7 331 911	915 081	5	Övertorneå	884 122	7 389 468	60
Kalix	Storöhamn	7 313 777	870 338	7	Överkalix-Svartbyn	851 240	7 371 437	46
Luleå	Orrbyn	7 332 089	823 115	15	Lakaträsk A	774 757	7 364 464	185
Piteå	Luleå airport	7 287 598	828 551	20	Vidsel	733 786	7 316 109	180
Byske	Pite Rönnskär	7 228 282	808 561	5	Fällfors	771 351	7 235 584	195
Skellefteå	Ursviken (T), Skellefteå (P)	7 191 095, 7 194 817	792 724, 782 685	5, 40	Klutmark	767 853	7 192 516	80
Robertsfors	Lövånger	7 152 682	804 483	21	Bygdsiljum	765 392	7 147 511	131
Sävar	Umeå airport	7 084 942	760 504	14	Vindeln -Sunnansjönäs	731 590	7 121 126	237
Hörnefors	Umeå airport	7 084 942	760 504	14	Vännäs	730 328	7 096 444	87
Nordmaling	Järnäsklubb	7 042 574	733 017	6	Nordmaling	722 692	7 057 349	4

Table A.3
Chronosequence specific parameters for the shore displacement curves. Landscape age can be calculated using the formula $T_{age} = a_0 + a_1 z + a_2 z^2$, where z corresponds to the elevation above sea level (m).

Chronosequence	a_0	a_1	a_2
Haparanda	244.26	122.16	−0.4037
Kalix	140.48	120.83	−0.4037
Luleå	165.42	118.61	−0.3890
Piteå	236.64	94.556	−0.2513
Byske	225.16	95.922	−0.2599
Skellefteå	169.63	90.864	−0.2288
Robertsfors	203.19	89.364	−0.2255
Sävar	421.07	82.713	−0.1818
Hörnefors	435.85	82.088	−0.1791
Nordmaling	426.63	81.157	−0.1746

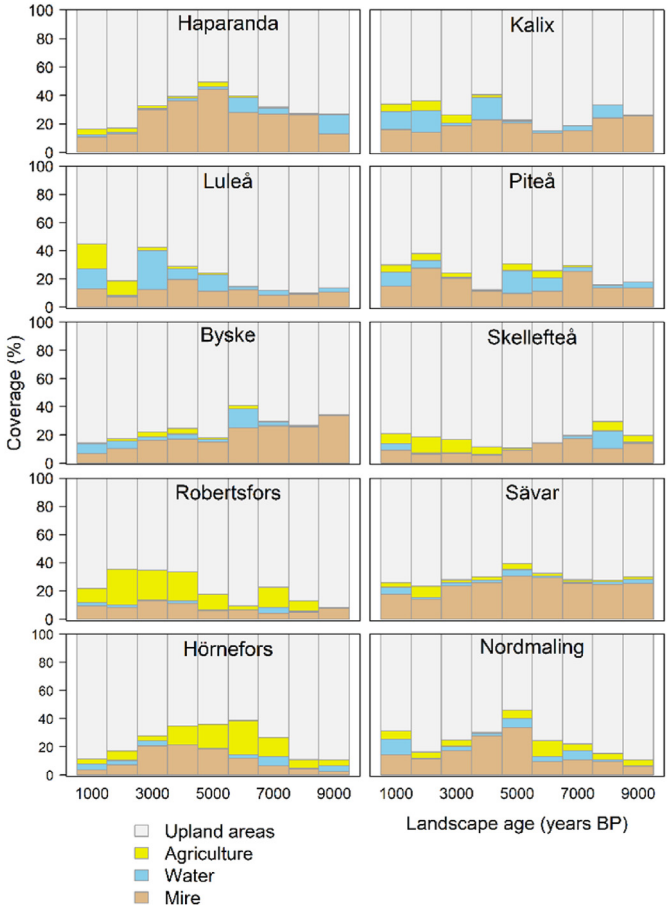

Fig. A.1. Land use coverage (%) variations in ten mire chronosequences across ages zones.

Table A.4
Kendall's rank correlation coefficients are based on the percentage of agriculture and residuals between the present mire coverage and the available land areas (mire % - available %) for moist and semi-moist areas respectively. Significance levels are indicated as: p = 0.1 (*), p = 0.05 (**) and p = 0.001 (***). In 5b. surface water was removed from the available areas and correlation coefficients, as well as p-values were calculated between the present coverage of agricultural land and the residuals in mire available land currently not covered by mires (mire % - available %).

Chronosequence	Mire drainage for agriculture	
	Moist areas	Semi-moist areas
Haparanda	–	−0.6
Kalix	−0.4*	−0.3
Luleå	−0.5*	−0.6*
Piteå	−0.6**	−0.9***
Byske	0.4	0.1
Skellefteå	−0.4	−0.3
Robertsfors	−0.1	−0.6***
Sävar	0.4	−0.1
Hörnefors	−0.5**	−0.4*
Nordmaling	−0.6**	−0.5**
All	< −0.01	<0.01

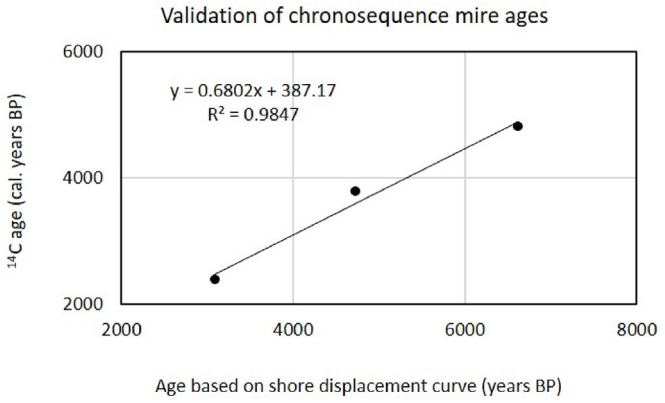

Fig. A.2. Comparison of land surface ages and calibrated ^{14}C ages (Klarqvist et al., 2001) for three mires from different chronosequences in the study area: Stor-Åmyran, Sjulsmyran and Rismyran from the Hörnefors, Sävar and Kalix chronosequences. Elevation based mire ages are linearly related to ^{14}C ages (R^2 = 0.98), although, in all mires the modelled mires ages are overestimating the actual ages (cal BP) with several hundreds of years.

References

Ågren, A.M., Hasselquist, E.M., Stendahl, J., Nilsson, M.B., Paul, S.S., 2022. Delineating the distribution of mineral and peat soils at the landscape scale in northern boreal regions. EGUsphere 1-23. https://doi.org/10.5194/egusphere-2000-79.

Ågren, A.M., Larson, J., Paul, S.S., Laudon, H., Lidberg, W., 2021. Use of multiple LIDAR-derived digital terrain indices and machine learning for high-resolution national-scale soil moisture mapping of the Swedish forest landscape. Geoderma 404, 115280. https://doi.org/10.1016/j.geoderma.2021.115280.

Almquist-Jacobson, H., Foster, D.R., 1995. Toward an integrated model for raised-bog development: theory and field evidence. Ecology 76, 2503–2516. https://doi.org/10.2307/2265824.

Berglund, Ö., Berglund, K., 2010. Distribution and cultivation intensity of agricultural peat and gyttja soils in Sweden and estimation of greenhouse gas emissions from cultivated peat soils. Geoderma 154, 173–180. https://doi.org/10.1016/j.geoderma.2008.11.035.

Beven, K.J., Kirkby, M.J., 1979. A physically based, variable contributing area model of basin hydrology/Un modèle à base physique de zone d'appel variable de l'hydrologie du bassin versant. Hydrol. Sci. Bull. 24, 43–69. https://doi.org/10.1080/02626667909491834.

Clark, P.U., Dyke, A.S., Shakun, J.D., Carlson, A.E., Clark, J., Wohlfarth, B., Mitrovica, J.X., Hostetler, S.W., McCabe, A.M., 2009. The last glacial maximum. Science 325, 710–714. https://doi.org/10.1126/science.1172873.

Clymo, R.S., Turunen, J., Tolonen, K., 1998. Carbon accumulation in peatland. Oikos 81, 368. https://doi.org/10.2307/3547057.

Conrad, O., Bechtel, B., Bock, M., Dietrich, H., Fischer, E., Gerlitz, L., Wehberg, J., Wichmann, V., Böhner, J., 2015. System for automated geoscientific analyses (SAGA) v. 2.1.4. Geosci. Model Dev. 8, 1991. https://doi.org/10.5194/gmd-8-1991-2015. –2007.

Ecke, F., Rydin, H., 2000. Succession on a land uplift coast in relation to plant strategy theory. Ann. Bot. Fenn. 37, 163–171.

Englund, G., Eriksson, H., Nilsson, M.B., 2013. The birth and death of lakes on young landscapes. Geophys. Res. Lett. 40, 1340–1344. https://doi.org/10.1002/grl.50281.

Foster, D.R., Jacobson, H.A., 1990. The comparative development of bogs and fens in central Sweden: evaluating the role of climate change and ecosystem development. Aquilo Ser Bot. 28, 15–26.

Foster, D.R., Wright, H.E., Jr., King, G.A., M.T., 1988. Bog development and landform dynamics in Central Sweden and South-eastern labrador, Canada. Br. Ecol. Soc. 76, 1164–1185. doi.org/10.2307/2260641.

Gallego-Sala, A.V., Charman, D.J., Harrison, S.P., Li, G., Prentice, I.C., 2016. Climate-driven expansion of blanket bogs in Britain during the Holocene. Clim. Past 12, 129–136. https://doi.org/10.5194/cp-12-129-2016.

Gorham, E., 1957. The development of peat lands. Q. Rev. Biol. 32, 145–166. https://doi.org/10.1007/s13398-014-0173-7.2.

Gorham, E., Lehman, C., Dyke, A., Janssens, J., Dyke, L., 2007. Temporal and spatial aspects of peatland initiation following deglaciation in North America. Quat. Sci. Rev. 26, 300–311. https://doi.org/10.1016/j.quascirev.2006.08.008.

Gorham, E., Lehman, C., Dyke, A., Clymo, D., Janssens, J., 2012. Long-term carbon sequestration in North American peatlands. Quat. Sci. Rev. 58, 77–82. https://doi.org/10.1016/j.quascirev.2012.09.018.

Graniero, P.A., Price, J.S., 1999. The importance of topographic factors on the

distribution of bog and heath in a Newfoundland blanket bog complex. Catena 36, 233–254. https://doi.org/10.1016/S0341-8162(99)00008-9.
Gunnarsson, U., Löfroth, M., 2009. Våtmarksinventeringen: Resultat Från 25 Års Inventeringar ; Nationell Slutrapport För Våtmarksinventeringen (VMI) I Sverige. Rapport/Naturvårdsverket. Naturvårdsverket, Stockholm.
Gunnarsson, U., Löfroth, M., Sandring, S., 2014. The Swedish Wetland Survey: Compiled Excerpts from the National Final Report, Rapport/Naturvårdsverket. Swedish Environmental Protection Agency, Stockholm.
Huikari, O., 1956. Primäärisen soistumisen osuudesta Suomen soiden synnyssä. Commun. Inst. For. Fenn. 46, 1–79.
Husen, E., Salma, S., Agus, F., 2014. Peat emission control by groundwater management and soil amendments: evidence from laboratory experiments. Mitig. Adapt. Strategies Glob. Change 19, 821–829. https://doi.org/10.1007/s11027-013-9526-3.
Ivanov, K.E., 1981. Water Movement in Mirelands. Academic Press Inc.(London) Ltd.
Joosten, H., 2003. Wise use of mires: background and principles, 239–250. https://doi.org/10.1080/11956860.1996.11682334.
Klarqvist, M., 2001. Peat growth and carbon accumulation rates during the Holocene in boreal mires. Dlss. Sveriges lantbruksuniv. Acta Univ. Agric. Sueciae Silvestria 1401–6230. http://urn.kb.se/resolve?urn=urn:nbn:se:slu:epsilon-p-107989.
Korhola, A., 1996. Initiation of a sloping mire complex in southwestern Finland: autogenic versus allogenic controls. Ecoscience 3, 216–222. https://doi.org/10.1080/11956860.1996.11682334.
Korhola, A., Ruppel, M., Seppä, H., Väliranta, M., Virtanen, T., Weckström, J., 2010. The importance of northern peatland expansion to the late-Holocene rise of atmospheric methane. Quat. Sci. Rev. 29, 611–617. https://doi.org/10.1016/j.quascirev.2009.12.010.
Korhola, A.A., 1994. Radiocarbon evidence for rates of lateral expansion in raised mires in southern Finland. Quat. Res. https://doi.org/10.1006/qres.1994.1080.
Kulczyński, S., 1949. Peat Bogs of Polesie. Academie Polonaise des Sciences et des Lettres, Cracovie.
Kutenkov, S.A., Kozhin, M.N., Golovina, E.O., Kopeina, E.I., Stoikina, N.V., 2018. Polygonal patterned peatlands of the White Sea islands. IOP Conf. Ser. Earth Environ. Sci. 138, 012010. https://doi.org/10.1088/1755-1315/138/1/012010.
Lafleur, P.M., Moore, T.R., Roulet, N.T., Frolking, S., 2005. Ecosystem respiration in a cool temperate bog depends on peat temperature but not water table. Ecosystems 8, 619–629. https://doi.org/10.1007/s10021-003-0131-2.
Lähteenoja, O., Reátegui, Y.R., Räsänen, M., Torres, D.D.C., Oinonen, M., Page, S., 2012. The large A mazonian peatland carbon sink in the subsiding P astaza-M arañón foreland basin. P eru. Glob. Change Biol. 18, 164–178.
Laine, A.M., Lindholm, T., Nilsson, M., Kutznetsov, O., Jassey, V.E.J., Tuittila, E., 2021. Functional diversity and trait composition of vascular plant and *Sphagnum* moss communities during peatland succession across land uplift regions. J. Ecol. 109, 1774–1789. https://doi.org/10.1111/1365-2745.13601.
Lane, C.R., Leibowitz, S.G., Autrey, B.C., LeDuc, S.D., Alexander, L.C., 2018. Hydrological, physical, and chemical functions and connectivity of non-floodplain wetlands to downstream waters: a review. JAWRA J. Am. Water Resour. Assoc. 54, 346–371. https://doi.org/10.1111/1752-1688.12633.
Lantmäteriet, 2020. Product Description: GSD-Property Map, Vector. https://www.lantmateriet.se/globalassets/geodata/geodataprodukter/produktlista/e_fastshmi.pdf.
Lindén, M., Möller, P., Björck, S., Sandgren, P., 2006. Holocene shore displacement and deglaciation chronology in Norrbotten, Sweden. Boreas 35, 1–22. https://doi.org/10.1080/03009480500359160.
Lindsay, R., Charman, D.J., Everingham, F., O'Reilly, R.M., Palmer, M.A., Rowell, T.A., Stroud, D.A., 1988. The Flow Country: the Peatlands of Caithness and Sutherland [WWW Document]. URL. http://www.jncc.gov.uk/page-4281. accessed 1.11.22.
Loisel, J., van Bellen, S., Pelletier, L., Talbot, J., Hugelius, G., Karran, D., Yu, Z., Nichols, J., Holmquist, J., 2017. Insights and issues with estimating northern peatland carbon stocks and fluxes since the Last Glacial Maximum. Earth Sci. Rev. 165, 59–80. https://doi.org/10.1016/j.earscirev.2016.12.001.
Loisel, J., Yu, Z., Beilman, D.W., Camill, P., Alm, J., Amesbury, M.J., Anderson, D., Andersson, S., Bochicchio, C., Barber, K., Belyea, L.R., Bunbury, J., Chambers, F.M., Charman, D.J., De Vleeschouwer, F., Fiałkiewicz-Kozieł, B., Finkelstein, S.A., Gałka, M., Garneau, M., Hammarlund, D., Hinchcliffe, W., Holmquist, J., Hughes, P., Jones, M.C., Klein, E.S., Kokfelt, U., Korhola, A., Kuhry, P., Lamarre, A., Lamentowicz, M., Large, D., Lavoie, M., MacDonald, G., Magnan, G., Mäkilä, M., Mallon, G., Mathijssen, P., Mauquoy, D., McCarroll, J., Moore, T.R., Nichols, J., O'Reilly, B., Oksanen, P., Packalen, M., Peteet, D., Richard, P.J., Robinson, S., Ronkainen, T., Rundgren, M., Sannel, A.B.K., Tarnocai, C., Thom, T., Tuittila, E.-S., Turetsky, M., Väliranta, M., van der Linden, M., van Geel, B., van Bellen, S., Vitt, D., Zhao, Y., Zhou, W., 2014. A database and synthesis of northern peatland soil properties and Holocene carbon and nitrogen accumulation. Holocene 24, 1028–1042. https://doi.org/10.1177/0959683614538073.
Loisel, J., Yu, Z., Parsekian, A., Nolan, J., Slater, L., 2013. Quantifying landscape morphology influence on peatland lateral expansion using ground-penetrating radar (GPR) and peat core analysis. J. Geophys. Res. Biogeosci. 118, 373–384. https://doi.org/10.1002/jgrg.20029.
MacDonald, G.M., Beilman, D.W., Kremenetski, K.V., Sheng, Y., Smith, L.C., Velichko, A.A., 2006. Rapid early development of circumarctic peatlands and atmospheric CH4 and CO2 variations. Science 314, 285–288. https://doi.org/10.1126/science.1131722.
Malmström, C., 1923. Degerö Stormyr: en botanisk hydrologisk och utvecklingshistorisk undersokning av ett nordsvenskt myrkomplex. Medd. Fran Statens Skogsforsoksanstalt 20.
Mathijssen, P.J.H., Väliranta, M., Korrensalo, A., Alekseychik, P., Vesala, T., Rinne, J., Tuittila, E.-S., 2016. Reconstruction of Holocene carbon dynamics in a large boreal peatland complex, southern Finland. Quat. Sci. Rev. 142, 1–15. https://doi.org/10.1016/j.quascirev.2016.04.013.
Mäukiläu, M., 1997. Holocene lateral expansion, peat growth and carbon accumulation on Haukkasuo, a raised bog in southeastern Finland. Boreas 26, 1–14. https://doi.org/10.1111/j.1502-3885.1997.tb00647.x.
Moor, H., Rydin, H., Hylander, K., Nilsson, M.B., Lindborg, R., Norberg, J., 2017. Towards a trait-based ecology of wetland vegetation. J. Ecol. 105, 1623–1635. https://doi.org/10.1111/1365-2745.12734.
Morris, P.J., Swindles, G.T., Valdes, P.J., Ivanovic, R.F., Gregoire, L.J., Smith, M.W., Tarasov, L., Haywood, A.M., Bacon, K.L., 2018. Global peatland initiation driven by regionally asynchronous warming. Proc. Natl. Acad. Sci. USA 115, 4851–4856. https://doi.org/10.1073/pnas.1717838115.
Murphy, P.N.C., Ogilvie, J., Meng, F.-R., White, B., Bhatti, J.S., Arp, P.A., 2011. Modelling and mapping topographic variations in forest soils at high resolution: a case study. Ecol. Model. 222, 2314–2332. https://doi.org/10.1016/j.ecolmodel.2011.01.003.
Nichols, J.E., Peteet, D.M., 2019. Rapid expansion of northern peatlands and doubled estimate of carbon storage. Nat. Geosci. 12, 917–921. https://doi.org/10.1038/s41561-019-0454-z.
Nordman, M., Peltola, A., Bilker-Koivula, M., Lahtinen, S., 2020. Past and future sea level changes and land uplift in the baltic sea seen by geodetic observations. In: International Association of Geodesy Symposia. Springer Berlin Heidelberg, Berlin, Heidelberg. https://doi.org/10.1007/1345_2020_124.
Ohlson, M., Okland, R.H., Nordbakken, J.-F., Dahlberg, B., 2001. Fatal interactions between Scots pine and spahgnum mosses in bog ecosystems. Oikos 94, 425–432.
Packalen, M.S., Finkelstein, S.A., McLaughlin, J.W., 2014. Carbon storage and potential methane production in the Hudson Bay Lowlands since mid-Holocene pear initiation. Nat. Commun. 5 (1), 1–8. https://doi.org/10.1038/ncomms5078.
Påsse, T., Daniels, J., 2015. Past Shore-Level and Sea-Level Displacements. Sveriges geologiska undersökning, Uppsala.
Paulson, A., Zhong, S., Wahr, J., 2007. Inference of mantle viscosity from GRACE and relative sea level data. Geophys. J. Int. 171, 497–508. https://doi.org/10.1111/j.1365-246X.2007.03556.x.
Payne, R.J., Malysheva, E., Tsyganov, A., Pampura, T., Novenko, E., Volkova, E., Babeshko, K., Mazei, Y., 2016. A multi-proxy record of Holocene environmental change, peatland development and carbon accumulation from Staroselsky Moch peatland, Russia. Holocene 26, 314–326. https://doi.org/10.1177/0959683615608692.
Pearsall, W.H., 1950. Mountains and Moorlands. Collins, New Naturalist, London.
Peregon, A., Uchida, M., Yamagata, Y., 2009. Lateral extension in Sphagnum mires along the southern margin of the boreal region, Western Siberia. Environ. Res. Lett. 4. https://doi.org/10.1088/1748-9326/4/4/045028.
Piilo, S.R., Korhola, A., Heiskanen, L., Tuovinen, J.P., Aurela, M., Juutinen, S., Marttila, H., Saari, M., Tuittila, E.S., Turunen, J., Väliranta, M.M., 2020. Spatially varying peatland initiation, Holocene development, carbon accumulation patterns and radiative forcing within a subarctic fen. Quat. Sci. Rev. 248. https://doi.org/10.1016/j.quascirev.2020.106596.
Pluchon, N., Hugelius, G., Kuusinen, N., Kuhry, P., 2014. Recent paludification rates and effects on total ecosystem carbon storage in two boreal peatlands of Northeast European Russia. Holocene. https://doi.org/10.1177/0959683614523803.
Quick, C., van der Velde, Y., Candel, J.H., Steinbuch, L., van Beek, R., Wallinga, J., 2022. Soil Geography and Landscape Group. In: Faded Landscape: Unravelling Peat Initiation and Lateral Expansion at One of NW-Europe's Largest Bog Remnants. Wageningen University & Research ([Manuscript submitted for publication]).
Ratcliffe, J.L., Creevy, A., Andersen, R., Zarov, E., Gaffney, P.P.J., Taggart, M.A., Mazei, Y., Tsyganov, A.N., Rowson, J.G., Lapshina, E.D., Payne, R.J., 2017. Ecological and environmental transition across the forested-to-open bog ecotone in a west Siberian peatland. Sci. Total Environ. 607–608, 816–828. https://doi.org/10.1016/j.scitotenv.2017.06.276.
Ratcliffe, J.L., Peng, H., Nijp, J.J., Nilsson, M.B., 2021. Lateral expansion of northern peatlands calls into question a 1,055 GtC estimate of carbon storage. Nat. Geosci. 14, 468–469. https://doi.org/10.1038/s41561-021-00770-9.
Romanov, V.V., 1968. Hydrographics of Bogs. Israel Programme for Scientific Translation, Jerusalem.
Ruppel, M., Väliranta, M., Virtanen, T., Korhola, A., 2013. Postglacial spatiotemporal peatland initiation and lateral expansion dynamics in North America and northern Europe. Holocene 23, 1596–1606. https://doi.org/10.1177/0959683613499053.
Rydin, H., Jeglum, J., Bennett, K., 2013. The Biology of Peatlands, 2e, second ed. Oxford university press.
Sannel, A.B.K., Kuhry, P., 2011. Warming-induced destabilization of peat plateau/thermokarst lake complexes. J. Geophys. Res. Biogeosci. 116. https://doi.org/10.1029/2010JG001635.
Sponseller, R.A., Blackburn, M., Nilsson, M.B., Laudon, H., 2018. Headwater mires constitute a major source of nitrogen (N) to surface waters in the boreal landscape. Ecosystems 21, 31–44. https://doi.org/10.1007/s10021-017-0133-0.
Stroeven, A.P., Hättestrand, C., Kleman, J., Heyman, J., Fabel, D., Fredin, O., Goodfellow, B.W., Harbor, J.M., Jansen, J.D., Olsen, L., Caffee, M.W., Fink, D., Lundqvist, J., Rosqvist, G.C., Strömberg, B., Jansson, K.N., 2016. Deglaciation of Fennoscandia. Quat. Sci. Rev., Spec. Iss.: PAST Gatew. (Palaeo-Arctic Spat. Temp.

Gatew.) 147, 91–121. https://doi.org/10.1016/j.quascirev.2015.09.016.
Sundberg, S., Hansson, J., Rydin, H., 2006. Colonization of Sphagnum on land uplift islands in the Baltic Sea: time, area, distance and life history. J. Biogeogr. 33, 1479–1491. https://doi.org/10.1111/j.1365-2699.2006.01520.
Tipping, R., 2008. Blanket peat in the Scottish Highlands: timing, cause, spread and the myth of environmental determinism. Biodivers. Conserv. 17, 2097–2113. https://doi.org/10.1007/s10531-007-9220-4.
Tiselius, A.K., Lundbäck, S., Lönnell, N., Jansson, R., Dynesius, M., 2019. Bryophyte community assembly on young land uplift islands – dispersal and habitat filtering assessed using species traits. J. Biogeogr. 46, 2188–2202. https://doi.org/10.1111/jbi.13652.
Tolonen, K., Turunen, J., 1996. Accumulation rates of carbon in mires in Finland and implications for climate change. Holocene 6, 171–178. https://doi.org/10.1177/095968369600600204.
Tuittila, E.-S., Juutinen, S., Frolking, S., Väliranta, M., Laine, A.M., Miettinen, A., Seväkivi, M.-L., Quillet, A., Merilä, P., 2013. Wetland chronosequence as a model of peatland development: vegetation succession, peat and carbon accumulation. Holocene 23, 25–35.
Turunen, C., Turunen, J., 2003. Development history and carbon accumulation of a slope bog in oceanic British Columbia, Canada. Holocene 13, 225–238. https://doi.org/10.1191/0959683603hl609rp.
Velde, Y. van der, Temme, A.J.A.M., Nijp, J.J., Braakhekke, M.C., Voorn, G.A.K., van, Dekker, S.C., Dolman, A.J., Wallinga, J., Devito, K.J., Kettridge, N., Mendoza, C.A., Kooistra, L., Soons, M.B., Teuling, A.J., 2021. Emerging forest–peatland bistability and resilience of European peatland carbon stores. Proc. Natl. Acad. Sci. USA 118. https://doi.org/10.1073/pnas.2101742118.
Walker, L.R., Wardle, D.A., Bardgett, R.D., Clarkson, B.D., 2010. The use of chronosequences in studies of ecological succession and soil development: chronosequences, succession and soil development. J. Ecol. 98, 725–736. https://doi.org/10.1111/j.1365-2745.2010.01664.x.
Weckström, J., Seppä, H., Korhola, A., 2010. Climatic influence on peatland formation and lateral expansion in sub-arctic Fennoscandia. Boreas 39, 761–769. https://doi.org/10.1111/j.1502-3885.2010.00168.x.
Yu, Z., Beilman, D.W., Jones, M.C., 2009. Sensitivity of northern peatland carbon dynamics to Holocene climate change. Carbon Cycl. N. Peatl. 184. https://doi.org/10.1029/2008GM000822, 55-69.
Yu, Z., 2011. Holocene carbon flux histories of the world's peatlands: global carbon-cycle implications. Holocene 21, 761–774. https://doi.org/10.1177/0959683610386982.
Yu, Z., Loisel, J., Brosseau, D.P., Beilman, D.W., Hunt, S.J., 2010. Global peatland dynamics since the last glacial maximum. Geophys. Res. Lett. 37, 1–5. https://doi.org/10.1029/2010GL043584.